# Effect of reaction time, heating and stirring rate on the morphology of HAp obtained by hydrothermal synthesis

Piotr Szterner[1] · Monika Biernat[1]

## Abstract

Hydroxyapatite (HAp) whiskers were prepared in reaction of calcium lactate pentahydrate and orthophosphoric acid. Synthesis were carried out in different conditions with using hydrothermal reactor. The benefit of the hydrothermal technique is the simple and precise control of the HAp crystals morphology, which is achieved by employing varying initial concentrations of starting reagents as well as different conditions of synthesis. The effect of time of synthesis, stirring and heating rate of the reaction on HAp morphology and composition was investigated. During the synthesis the following experimental parameters were varied independently: time of synthesis (3, 5, 7 h), stirring rate (0, 62.5, 125, 250, 500, 750 rpm), the reaction heating rate (0.2, 0.5, 0.7, 1.0, 1.5, 2.5 °C min$^{-1}$). All syntheses were carried out with the constant molar Ca/P ratio of 1.67 in starting solutions, which is equivalent to that of stoichiometric HAp. The Ca$^{2+}$ ion concentrations in starting solutions for synthesis were 0.05 and 0.1 mol dm$^{-3}$. Syntheses were carried out under 20 bar. The obtained products were characterized using different method like XRD, SEM, and FTIR. It was shown that the significant majority of samples prepared were identified as pure HAp.

**Keywords** Thermal behaviour · Hydroxyapatite whiskers · Calcium lactate pentahydrate · Hydrothermal synthesis

## Introduction

Calcium phosphates (CaPs) biomaterials are one of the most promising materials for applications in bone replacement or regeneration due to their excellent biological properties and similarity to the mineral component of the bone [1, 2, 3].

Across all various bioactive CaPs, hydroxyapatite (HAp) is the most widely used ceramic for bone tissue repair and reconstruction [4]. HAp is similar in composition to the mineral component of bone and teeth. Due to similarity HAp has been considered as one of the most bioactive and biocompatible materials for dental and biomedical applications [5].

Thanks to the distinguished properties such as bioactivity, biocompatibility, and osteoconductivity, HAp plays an important role [6, 7]. As a result of their biological activity and special adsorbability towards different ions and organic particles, hydroxyapatite has found application not only as artificial bones, scaffolds or bone filler for tissue engineering [7] but also as drug delivery carriers (like antibiotics, hormones, growth factors, antibacterial, anti-anflammatory, bone regenerative drugs) [8, 9], bioimaging [10], catalysts or catalysts carrier [11, 12], remineralizing agent in toothpastes [13], orthopaedic and dental implant coating [14] and adsorbents [15]. Also, nanocomposites derived from magnetic hydroxyapatite can be obtained by a variety of method [16].

For many of the above-mentioned applications fibrous materials seem to be interesting due to their high surface area and resemblance to the fibrous structure at bone [17]. Moreover, reinforcement by fibres or whiskers has been considered as an effective way of improving mechanical properties [18, 19]. In comparison with most available bio-inert fibres or whiskers, the most promising reinforcements seems to be CaP-based materials as a results of their good bioactivity and biocompatibility [5, 20]. Hence, HAp whiskers may be effective in improving both mechanical performance and adhesion to bone and implant surfaces [5]. Interesting application of whiskers is also possibility to use to fabricate a free-standing membrane with exhibiting a unique bird

✉ Piotr Szterner
  piotr.szterner@icimb.lukasiewicz.gov.pl

[1] Biomaterials Research Group, ŁUKASIEWICZ Research Network - Institute of Ceramics and Building Materials, Center of Ceramic and Concrete in Warsaw, Cementowa 8, 31-983 Cracov, Poland

nest-like microstructure for separate the Au nanoparticles (3 nm) [22].

Hydroxyapatite whiskers can be prepared by a variety of methods [17, 22, 23, 24, 25, 26, 27, 28, 29, 30], amongst which are the wet chemical routes, including homogeneous precipitation [22, 23], decomposition of Ca-chelate [24, 25], dissolution–reprecipitation [26], hydrolysis with microwave heating [27], and the hydrothermal method [28, 29, 30]. Also, submicron hydroxyapatite fibres were fabricated by electroblowing [17]. Well-crystallized whiskers can also be easily obtained by various facile hydrothermal methods from aqueous solution containing calcium and phosphate. Hydrothermal method is a useful method of preparing large and non-aggregated crystals and whiskers with high purity, low dislocation density, controllable aspect ratio, and high crystallinity [5, 31].

The hydrothermal method can be also used for obtaining various derivatives of phosphate like as zirconium phosphate [32].

Recently, calcium lactate pentahydrate and creatine phosphate disodium salt tetrahydrate were used for microwave hydrothermal synthesis of hierarchical mesoporous structured hydroxyapatite microflowers [33].

Morphology and phase content of product obtained during hydrothermal synthesis may depend on many parameters like initial $Ca^{+2}$ ion concentration, molar Ca/P ratio, temperature and pressure of reactions, pH of solutions [24, 34, 35, 36, 37]. Nevertheless, it turns out that other factors, such as time of synthesis, stirring rate, the reaction heating rate can also have a great influence on morphology and phase content on the synthesized hydroxyapatite particles [38].

Also, the effect of the reaction temperature on the morphology of nanoHAp was investigated [39]

The purpose of this work was to obtained HAp whiskers directly from reaction between calcium lactate pentahydrate and orthophosphoric acid. As this reaction is based on chelate decomposition, the effect of different: reaction time, reaction heating rate and stirring rates on HAp morphology and phase content was investigated in detail. Received products were analysed by scanning electron microscope (SEM), Fourier transform infrared spectroscopy (FTIR) and X-ray diffraction method (XRD). In addition, the results of thermal analysis of the obtained products were presented along with a discussion of the presented reaction processes.

The observed dependencies in this study remain in correlation and complement the results presented in our earlier work describing the influence of: reagents concentrations, solution pH, and reaction temperature and pressure on the morphology and phase content of HAp obtained in hydrothermal synthesis between calcium lactate pentahydrate and orthophosphoric acid [40].

With regard to the literature review, no data about the hydrothermal synthesis with the direct use of calcium lactate pentahydrate and orthophosphoric acid have been published. To our knowledge, in this work for the first time the effect of reaction condition on whiskers morphology and their phase composition during decomposition of calcium lactate pentahydrate chelates was presented.

The advantage of the presented method is the facile but precise control of the HAp crystals morphology and great product purity which is necessary for biomedical utilizations.

Also, the advantage of this synthesis is possibility to obtain product of different morphology like whiskers and hexagonal rods depending on the reaction conditions. The obtained Hap of different morphology can be use likes filler in composites applied in biomaterials.

## Experimental

### Chemicals

The main substrates for the synthesis were calcium lactate pentahydrate $C_6H_{10}CaO_6 \cdot 5H_2O$ and orthophosphoric acid $H_3PO_4$. Both compounds were pure p.a and obtained from Chempur®, Poland.

### Preparation

Hydroxyapatite have been prepared by the hydrothermal method. Synthesis were carried out in various conditions with using a stainless steel reactor (Büchiglasuster®, miniclave steel type 3/300 mL, 100 bar) enabling heating of aqueous solutions to high temperatures up to 200 °C.

HAp products were synthesized from aqueous solutions containing calcium lactate pentahydrate and orthophosphoric acid. The molar Ca/P ratio in the solution of 1.67, corresponding to stoichiometric Hap, was respected.

The calcium lactate pentahydrate was dissolved in deionized water, to make a homogeneous solution and then a solution of orthophosphoric acid was added. The mixed solutions were poured into a reaction vessel and heated at temperature set value. During hydrothermal synthesis, the temperature and pressure inside of reactor were regularly monitored.

Upon completion of each reaction the vessel was cooled to ambient temperature (~25 °C) overnight. The product was then filtered off, washed quickly with deionized water four times, and finally dried in air in the laboratory dryer at 100 °C for at least 6 h. The description of used temperature controller, thermocouple and pH measurement is presented in paper [40].

## Characterization

### Scanning electron microscopy (SEM)

Microscopic observations, sample morphology and local microstructure analysis of the obtained whiskers were performed using a field emission scanning electron microscope (Nova NanoSEM200, FEI). Width and length of the obtained whiskers were determined on the basis of microscopic images using measurement and annotation functions on the sample area. A detailed description of SEM used is presented in the work [40].

### X-ray diffraction method (XRD)

The phase composition products obtained by hydrothermal synthesis were analysed by Bragg- Brentano X-ray diffraction method (XRD) on a Bruker-AXS D8 DAVINCI diffractometer designed for a copper anode tube.

Crystalline phases were identified in DIFFRACplus EVA-SEARCH software with recorded diffraction patterns and standards from ICDD PDF-2, PDF-4 + 2016 databases and the Crystallography Open Database (COD). Quantitative analysis was carried out using the Rietveld method in the Topas v.50 software, based on published crystalline structures (COD). A detailed description of the methods applied in the present study can be found in paper [40].

### Fourier transform infrared spectroscopy (FTIR spectroscopy)

Functional groups of the samples were identified by FTIR. Measurements of absorbance were made using a TENSOR 27 (BRUKER) equipped with a DLaTGS detector. The analysis was performed in the wavelength range from $400\ cm^{-1}$ to $4000\ cm^{-1}$. The samples were prepared as pressed pellet shape KBr moulds.

### Thermal analysis

Phase changes and thermal decomposition of hydroxyapatite were studied by thermogravimetric analysis (TG) and differential thermal analysis (DTA).

Thermal analysis was carried out on a STA 449 Jupiter F1 apparatus from Netzsch (Gerätebau GmbH, Germany).

Each sample mass was about 20 mg. Before measurement, each sample was ground into fine powder using an agate mortar and pestle and next it was dried in laboratory dryer by 19 h in 90 °C. TG–DTA measurements carried out in the range of temperature from 25 to 1550 °C with a heating rate of $10\ °C\ min^{-1}$ in argon atmosphere (flow rate: $70\ mL\ min^{-1}$). For each sample carried out separate measurement corrective on the empty crucible.

## Results

### Synthesis

In the case of the attempts to synthesize HA whiskers using chemical methods that decompose chelates, described earlier in the literature, an inability to replicate the whiskers morphology (e.g. shape factor) was observed. Further research revealed that the heating rate of the reaction is a critical parameter, infrequently described in the published works [38]. Since the synthesis between calcium lactate pentahydrate and orthophosphoric acid can be regulated by the controlled release of calcium into the solution, we set out to study whisker morphology and phase composition as a function of heating rate. We investigated also mixing speed and the effect of different reaction time on the products morphology.

At the time of the reaction the following searching factors were changed independently: time of the synthesis (3 h,5 h,7 h), the stirring rate (0 rpm, 62.5 rpm, 125 rpm, 250 rpm, 500 rpm, 750 rpm), the reaction heating rate ($2.5\ °C\ min^{-1}$, $1.5\ °C\ min^{-1}$, $1.0\ °C\ min^{-1}$, $0.7\ °C\ min^{-1}$, $0.5\ °C\ min^{-1}$, $0.2\ °C\ min^{-1}$). The $Ca^{2+}$ ions concentrations in starting synthesis solutions were $0.05\ mol\ dm^{-3}$. The influence of the reaction time on the morphology of the obtained products was tested at two $Ca^{2+}$ ions concentrations in starting synthesis solutions of $0.05\ mol\ dm^{-3}$ and $0.1\ mol\ dm^{-3}$. The molar Ca/P ratio in starting solutions was 1.67. The influence of chosen parameters on the morphology and phase composition of the synthesized products is shown in Table 1.

### The effect of heating rate on the obtained products character

The results and conditions of synthesis performed in a temperature of 200 °C under a pressure of 20 bar for starting solutions with $Ca^{2+}$ ion concentration of $0.05\ mol\ dm^{-3}$, with the reaction heating rate: 2.5, 1.5, 1.0, 0.7, 0.5, $0.2\ °C\ min^{-1}$ were shown in Table 1 (I), whereas SEM micrographs of the received products were presented in Fig. 1. The diffraction patterns of products obtained with the reaction heating rate 2.5, 1.5, 1.0 and $0.7\ °C\ min^{-1}$ can be allotted to a pure crystalline hydroxyapatite phase, which is in an excellent agreement with the reference data (PDF no. 00–009-0432). No peaks for any other phases were

**Table 1** The influence of hydrothermal synthesis conditions on the morphology and phase composition of the obtained products

| Ca²⁺ Concentration mol L⁻¹ | pH before synthesis | pH after synthesis | Time of synthesis/h | Temperature of synthesis/°C | Pressure/bar | Stirring rate/rpm | The reaction heating rate °C min⁻¹ | Length/μm | Width/μm | Phase Composition (form) |
|---|---|---|---|---|---|---|---|---|---|---|
| *Different heating rate of synthesis (I)* | | | | | | | | | | |
| 0.05 | 3.91 | 3.30 | 5 | 200 | 20 | 250 | **2.5** | 58.4–111.1 | 2.0–3.0 | Whiskers (Hap) |
| | 4.05 | 3.44 | | | | | **1.5** | 28.0–61.9 | 1.8–5.9 | Hexagonal rods (Hap) |
| | 4.08 | 3.05 | | | | | **1.0** | 22.2–41.8 | 2.3–4.5 | Hexagonal rods (Hap) |
| | 3.97 | 3.12 | | | | | **0.7** | 11.1–24.4 | 2.2–2.6 | Hexagonal rods (Hap) |
| | 3.99 | 3.29 | | | | | **0.5** | 15.3–34.5 | 2.7–4.5 | 98% HAp (hexagonal rods) + 2% β-TCP |
| | 3.96 | 3.31 | | | | | **0.2** | 22.3–38.6 | 2.7–4.5 | 92.8% HAp (hexagonal rods) + 7.2% β-TCP |
| *Different time of synthesis (II)* | | | | | | | | | | |
| 0.05 | 4.08 | 3.42 | **3** | 200 | 20 | 250 | 2.5 | 10.0–22.0 | 2.0–3.0 | Hexagonal rods (Hap) |
| | 3.91 | 3.30 | **5** | | | | | 58.4–111.1 | 2.0–3.0 | Whiskers (Hap) |
| | 4.08 | 3.59 | **7** | | | | | 27.8–69.5 | 1.5–5.5 | Hexagonal rods (Hap) |
| 0.1 | 3.69 | 2.78 | **3** | 200 | 20 | 250 | 2.5 | 13.6–25.0 | 1.8–5.0 | Hexagonal rods (Hap) |
| | 4.13 | 3.21 | **5** | | | | | 30.2–37.8 | 2.2–4.5 | Hexagonal rods (Hap) |
| | 3.94 | 3.16 | **7** | | | | | 21.1–56.8 | 2.2–5.5 | Hexagonal rods (Hap) |
| *Different stirring rate (III)* | | | | | | | | | | |
| 0.05 | 3.93 | 2.75 | 5 | 200 | 20 | **0** | 2.5 | 22.2–38.6 | 1.0–4.5 | Whiskers and hexagonal rods (Hap) |
| | 3.92 | 3.05 | | | | **62.5** | | 52.1–83.6 | 2.2–4.5 | Whiskers and hexagonal rods (Hap) |
| | 3.85 | 3.17 | | | | **125** | | 47.3–75.2 | 2.2–4.5 | Whiskers and hexagonal rods (Hap) |
| | 3.91 | 3.30 | | | | **250** | | 58.4–111.1 | 2.0–3.0 | Whiskers (Hap) |
| | 3.92 | 3.75 | | | | **500** | | 15.9–45.5 | 2.7–4.5 | Hexagonal rods (Hap) |
| | 4.22 | 3.68 | | | | **750** | | 17.4–25.7 | 1.8–3.2 | Whiskers (Hap) |

Thus bold refers to hydrothermal synthesis conditions
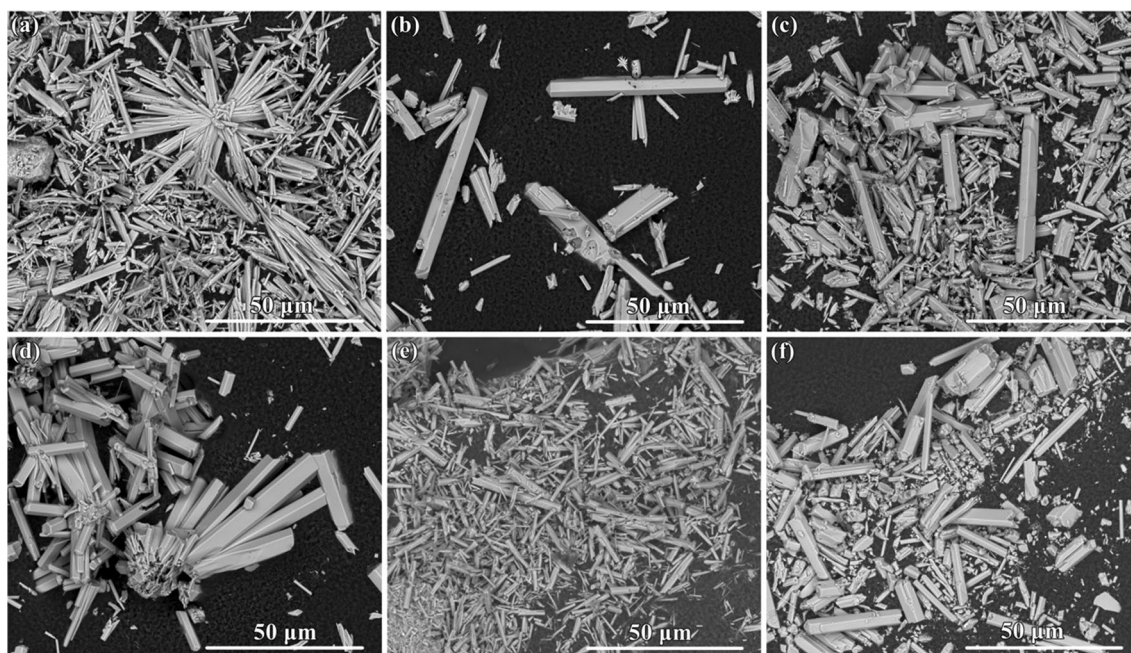
**Fig. 1** SEM images of products synthesized in hydrothermal synthesis carried out at: 200 °C, 20 bar, 5 h, $Ca^{2+}$ ion concentration of 0.05 mol $dm^{-3}$, for reaction heating rate: **a** 2.5 °C $min^{-1}$ (58.4–111.1 μm), **b** 1.5 °C $min^{-1}$ (28–61.9 μm), **c** 1.0 °C $min^{-1}$ (22.2–41.8 μm), **d** 0.7 °C $min^{-1}$ (11.1–24.4 μm), **e** 0.5 °C $min^{-1}$ (15.3–34.5 μm), **f** 0.2 °C $min^{-1}$ (22.3–38.6 μm) (magnification of 2500×)

determined for this specimen. However, when the reaction heating rate is 0.5 or 0.2 °C $min^{-1}$, also the peaks of β-TCP appeared. The peaks obtained were compared with standard references in PDF file available in software for whitlockite, β-TCP (no. 00–055-0898).

The phase composition of the obtained products was confirmed by FTIR. Figure 2 presents the characteristic FT-IR spectra of three specimens obtained with different reaction heating rate of synthesis. For sample a, b, c the reaction heating rate was 2.5 °C $min^{-1}$, 0.5 °C $min^{-1}$, 0.2 °C $min^{-1}$, respectively. Analysis of the chemical structure using FTIR shows that for HAp and β–TCP, the peaks in range 562–604 $cm^{-1}$ and 962–1094 $cm^{-1}$ can be assigned to the phosphate group ($PO_4$) [41, 42, 43]. Bands in range 562–604 $cm^{-1}$ correspond to anti- symmetric P-O bending triply degenerate ($\nu_4$). Absorbance band in range 962–969 $cm^{-1}$ is assigned to symmetric P-O stretching ($\nu_1$). Whereas bands in range 1029–1094 $cm^{-1}$ correspond to anti-symmetric P-O stretching triply degenerate ($\nu_3$). The weak peak at range of 473–476 $cm^{-1}$ is component of the doubly degenerated bending mode, ($\nu_2$) of the O–P–O bonds of the phosphate group $PO_4$. The characteristic peak 3571 $cm^{-1}$ was assigned to the stretching mode of hydroxyl group ($OH^-$), while the bending vibrational mode of hydroxyl group occurred in a peak at 634 $cm^{-1}$ appear in HAp samples. It is apparent negligible shift of this band at 635 $cm^{-1}$ and at 636 $cm^{-1}$ in dependence of decrease of content of HAp phase. Besides, this peak cannot be seen in TCP since chemical structure of TCP lack $OH^-$ group. It is worthy of note that the broad

absorption peak at about 3400 $cm^{-1}$ and transmission band at 1647–1614 $cm^{-1}$ is allotted to adsorbed water molecules [44, 45]. The peaks associated to gaseous $CO_2$ (dissolved) are detectable in range 2360–2366 $cm^{-1}$ and 2341–2344 $cm^{-1}$ [46]. Thus, in FTIR pattern of BCP, in addition to peaks of $PO_4^{3-}$ and $CO_3^{2-}$, the peaks of OH- groups can also be visible [43].

Reaction heating rate of hydrothermal synthesis also influences HAp morphology. HAp in the shape of whiskers was obtained during the synthesis with the heating rate of 2.5 °C $min^{-1}$ (Fig. 1a). HAp in the form of hexagonal rods was obtained during reaction with the heating rate of 1.5 °C $min^{-1}$ and 1.0 °C $min^{-1}$ (Fig. 1b, 1c). HAp in the form of bundles of hexagonal rods were received during reaction with the heating rate of 0.7 °C $min^{-1}$ (Fig. 1d). The hexagonal rods consisted of HAp (98%) and calcium phosphate (2%) were obtained during reaction with the heating rate of 0.5 °C $min^{-1}$ (Fig. 1e). The hexagonal rods, consisted of HAp (92.8%) and calcium phosphate (7.2%) were obtained during reaction with the heating rate of 0.2 °C $min^{-1}$ (Fig. 1f).

## The influence of the reaction time on the synthesized products character

The dependence of phase composition and dimensions of the received products on the reaction time was determined for reaction performed during 3, 5 and 7 h, at a temperature
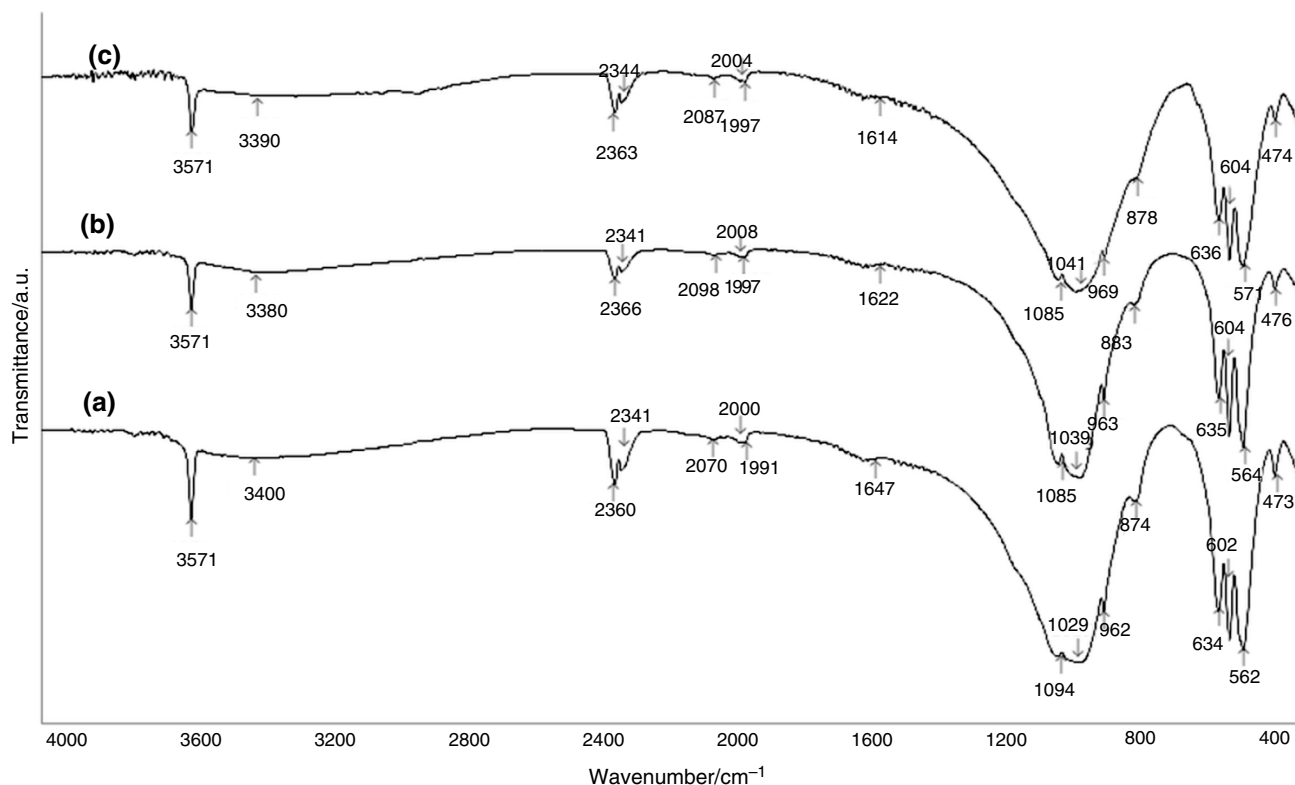
**Fig. 2** FT-IR spectra of (a) 100% HAp, (b) BCP 98% HAp-2% β-TCP, (c) 92.8% HAp-7.2% β-TCP

of 200 °C, in a pressure p = 20 bar, for two starting solution concentrations of $Ca^{2+}$ equal to 0.05 mol $dm^{-3}$ and 0.1 mol $dm^{-3}$. The results and conditions of the synthesis were presented in Table 1 (II). As can be seen, pure HAp was the product of all the synthesis, regardless of the reaction time. For the reaction with $Ca^{2+}$ ion concentration of 0.05 mol $dm^{-3}$ the phase composition was confirmed also by FTIR spectra of the products of synthesis (Fig. 3).

The morphology of the obtained products was also presented on SEM images (Fig. 4). As can be seen, the form of the obtained products changed with the change in reaction time. The smallest HAp particles in form of short hexagonal rods (length 10–22 μm) were obtained during 3 h synthesis. For the 5 h synthesis HAp in form of long whiskers created characteristic sheaf bundles (length 58.4–111.1 μm) was obtained. The further increase in reaction time affects the obtaining of HAp particles in form of hexagonal rods again with significant smaller length (27.8–69.5 μm).

As shown in Table 1 (II) for the reaction with $Ca^{2+}$ ion concentration of 0.1 mol $dm^{-3}$, the reaction products are received in the same shape (hexagonal rods) for various reaction times. As the reaction time increases, the length of the obtained particles also increases.

## The effect of stirring rate on the obtained products character

Stirring rate during hydrothermal synthesis has significant impact on HAp morphology [19]. The effect of stirring rate on phase composition and morphology of the obtained products was determined for synthesis performed at 200 °C, under 20 bar, for starting solution concentration of $Ca^{2+}$ = 0.05 mol $dm^{-3}$ and with stirring rate of 0 rpm, 62.5 rpm, 125 rpm, 250 rpm, 500 rpm and 750 rpm. Reaction parameters and the obtained results were presented in Table 1 (III). The products morphologies were shown in Fig. 5. During the reaction without stirring (Fig. 5 (a)), HAp in the form of as well thin whiskers agglomerates as hexagonal rods was obtained. The use of slow mixing (stirring rate of 62.5 rpm) during the process resulted in obtaining of morphologically more homogeneous product, mostly in the form of longer whiskers with a little amount of hexagonal rods. The most homogeneous product and the longest whiskers (40–110 μm) in sheaf bundles form were obtained for stirring rate of 250 rpm. The further increase in stirring rate up to 500 rpm and 750 rpm resulted in the formation of short hexagonal rods and short whiskers as reaction products, respectively.
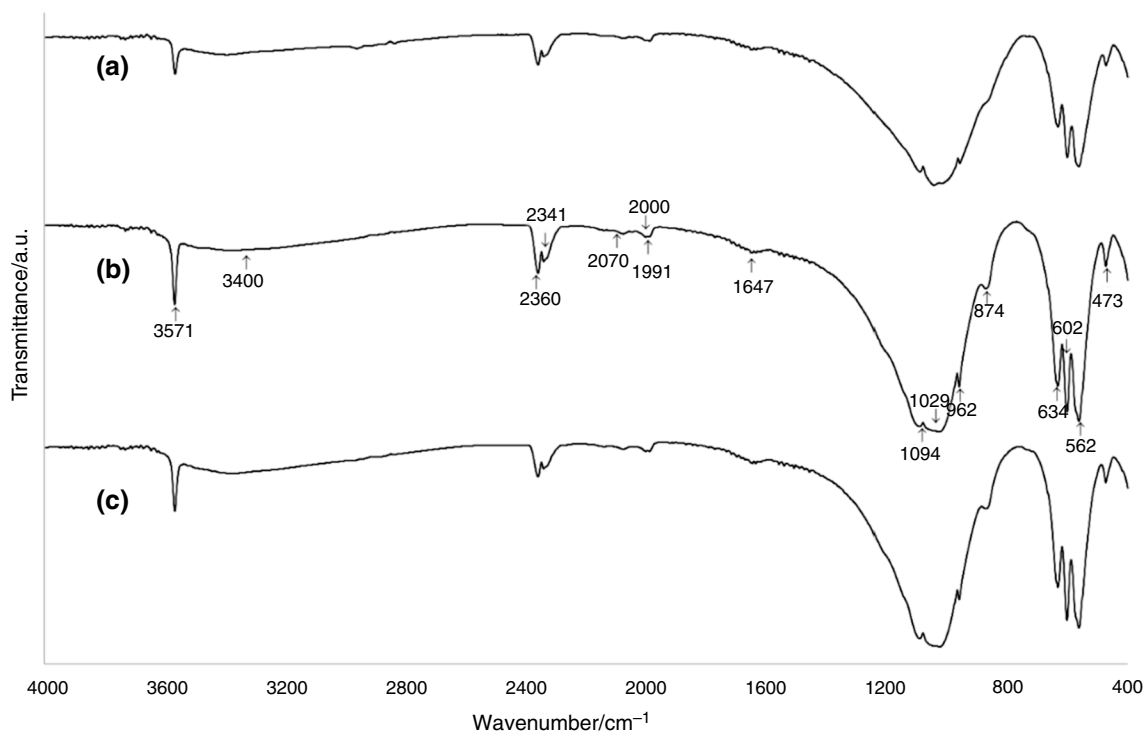
**Fig. 3** FTIR spectra of products obtained in time of: (a) 3, (b) 5 and (c) 7 h, at a temperature of 200 °C, and pressure of 20 bar, for $Ca^{2+}$ ion concentration of 0.05 mol $dm^{-3}$

## Thermal analysis

For two samples of HAp obtained during hydrothermal reaction with calcium lactate pentahydrate and orthophosphoric acid, thermal stability tests were carried out. The selected products were formed in a reaction conducted using the same concentrations of $Ca^{2+}$ ions, under the same conditions (200 °C, 20 bar) but at different reaction times (5 h and 3 h). Figure 6 shows DTA/TG, DTG/TG and DTA/DTG plots obtained during the tests. There are characteristic broad exothermic peaks in range of 400–1100 °C on the DTA plots for both tested products. There are also three regions of mass loss visible on the plots.

The first region of mass loss occurs in temperature range of 400–600 °C. For a 3 h synthesis the sample mass decreases by 0.42% in range of temperature 424–610 °C, whereas for a 5 h synthesis the sample mass decreases by 0.72% in range of temperature 374–632 °C. The peaks for a 3 and 5 h synthesis are visible on DTG plots at 571.3 °C and 590.0 °C, respectively.

The second region of mass loss occurs around 800 °C. For a 3 h synthesis the sample mass decreases by 1.0% in range of temperature 610–882 °C, whereas for a 5 h synthesis the sample mass decreases by 0.74% in range of temperature 632–890 °C. For a 3 and 5 h synthesis the peaks at 824.7 °C and 834.5 °C, respectively, are visible on DTG plots.

The last region of mass loss occurs around 890–1350 °C. For a 3 h synthesis the sample mass decreases by 1.10% in range of temperature 882–1345 °C, whereas for a 5 h synthesis the sample mass decreases by 0.74% in range of temperature 890–1364 °C.

To characterize products created during thermal analysis, the phase analysis of the residue from the sample subjected to thermal analysis was carried out. Figure 7 shows the XRD patterns of the sample before thermal analysis (HAp obtained in the hydrothermal reaction while maintaining the $Ca^{2+}$ concentration equal to 0.1 mol $dm^{-3}$ and conditions of 200 °C, 20 bar, in time of 3 h) and of this sample after thermal analysis carried out in range of 25 °C -1550 °C. The signals on diffraction pattern for the starting sample before thermal analysis are consistent with signals of standard pattern of HAp (PDF no.09–0432), suggesting the presence of single phase HAp in the sample. All the diffraction peaks for sample obtained after heating are identical with signals characteristic for alfa-calcium phosphate ($\alpha$ -$Ca_3(PO_4)_2$,$\alpha$-TCP) (COD no. 2106194) [47] and tetracalcium phosphate (TTCP, $Ca_4(PO_4)_2O$, COD no. 9011144) [48] what is consistent with literature data [49, 50, 51].
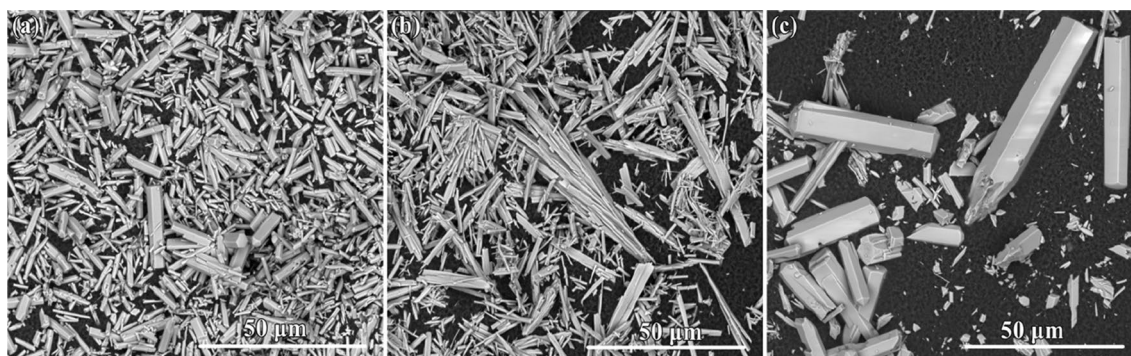
**Fig. 4** SEM images at 2500× magnification of products of hydrothermal synthesis (20 bar, 200 °C) for: **a** 3 h, $Ca^{2+}$ concentration 0.05 mol $dm^{-3}$, **b** 5 h, $Ca^{2+}$ concentration 0.05 mol $dm^{-3}$, **c** 7 h, $Ca^{2+}$ concentration 0.05 mol $dm^{-3}$
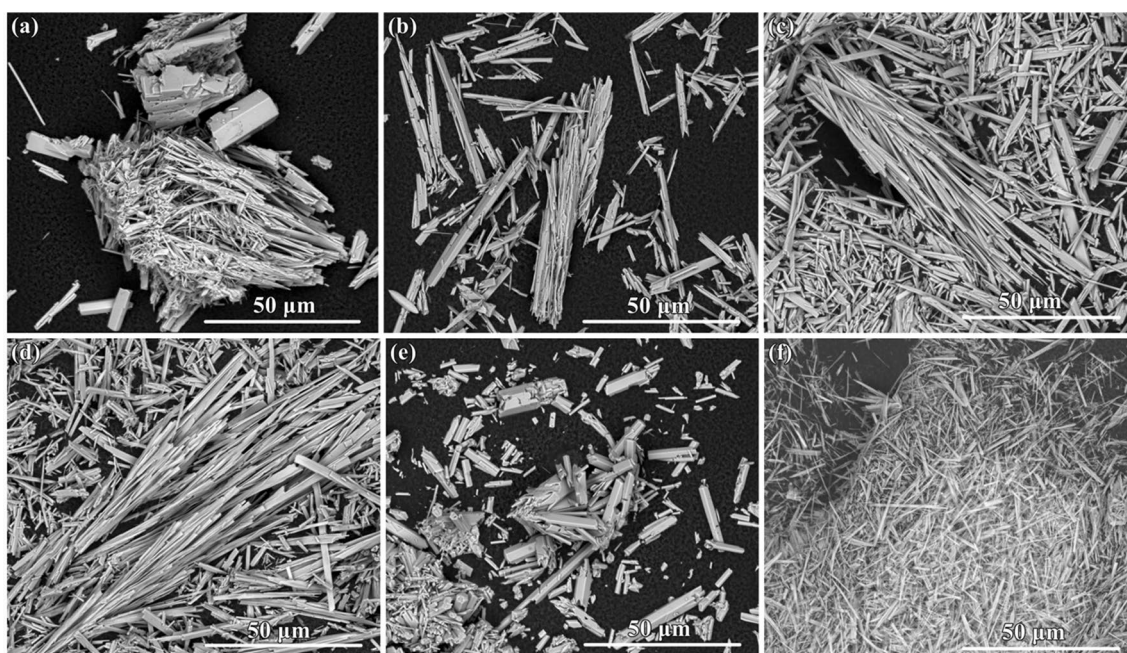


**Fig. 5** SEM images at 2500× magnification of products of hydrothermal synthesis (200 °C, 20 bar, 5 h, $Ca^{2+}$ concentration 0.05 mol $dm^{-3}$) for stirring rate in rpm: **a** 0, **b** 62.5, **c** 125, **d** 250, **e** 500 and **f** 750

## Discussion

### The influence of process reaction on properties of the obtained products

The morphology of HAp particles obtained during hydrothermal synthesis is affected among others by the heating rate of the reaction mixture. This is especially noticeable for reactions involving chelate decomposition. According to our observations, the various heating rates let receive various shapes and dimensions of HAp particles (Table 1). For high heating rates (2.5 °C $min^{-1}$), sheaf-like particles are formed, and for lower heating rates, well-developed HAp crystals in the shape of hexagonal rods can be seen. According to scientific papers data [38] the number of powder particles decreases with decreased heating rate. This probably allows in our synthesis the particles to grow slowly in a certain plane and formation of well-formed crystals and form of hexagonal rods. Moreover, according to published works data the mean length of whiskers increases and the mean width of whisker decreases with decreased heating rate [38]. However, our results remain the opposite to these data and we stated that dimensions of the obtained particles are strictly connected with particles forms. For HAp in hexagonal form both the length and the width of particles increased with decreased heating rate and the biggest dimensions were for the heating rate of 0.7 °C $min^{-1}$.

**Fig. 6** Thermal analysis of HAp synthesised by hydro-thermal method (200 °C, 20 bar, calcium concentration $Ca^{2+} = 0.2$ mol dm$^{-3}$, reaction time: (a) 5 h, (b) 3 h): **A** DTA/TG plots, **B** DTG/TG plots, **C** DTA/DTG plots
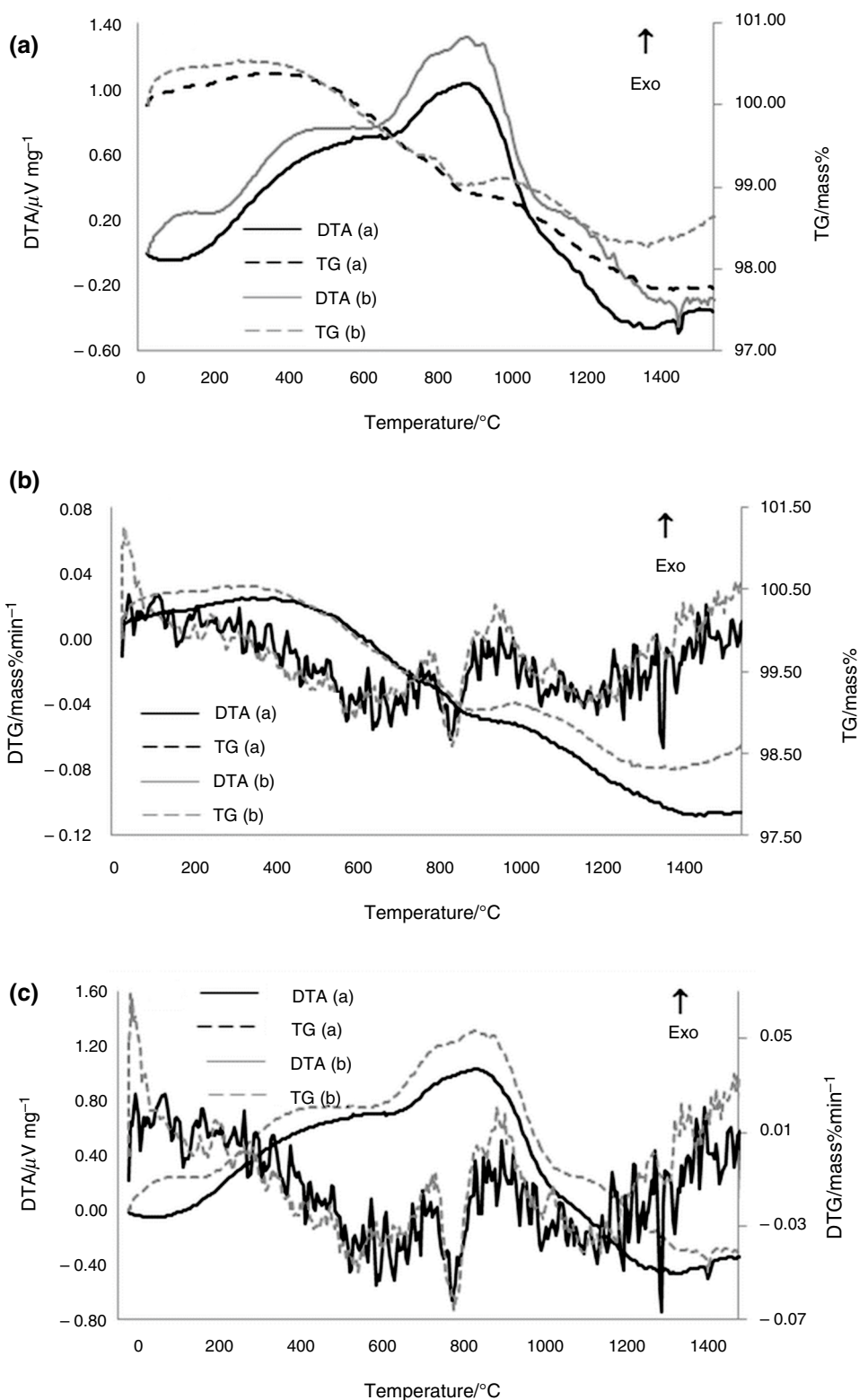
From the results received and the data presented in Table 1 it can be deduced that the results received are impacted by many factors at the same time. For instance, the dimensions of the obtained particles cannot be related solely for the sole change in $Ca^{2+}$ ion concentration or reaction time. The form of molecules formed in the in situ reaction plays a great role. Some concentrations, reaction time or heating rate are deficient to receive well-formed molecules,

**Fig. 7** The XRD patterns of sample HAp synthesised by hydrothermal method (200 °C, 20 bar), for calcium concentration $Ca^{2+} = 0.2$ mol dm$^{-3}$, during 3 h before and after thermal analysis (TA)
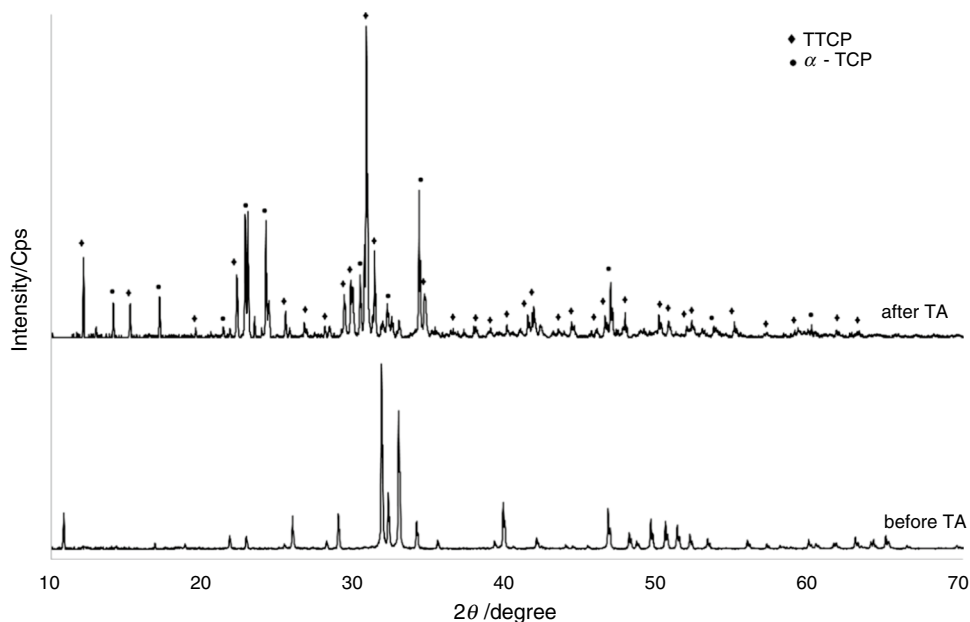


## Thermal analysis
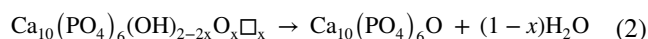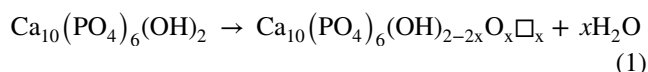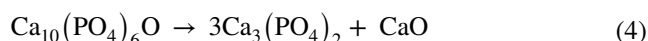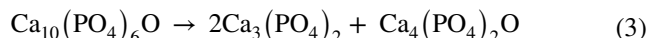
High temperature processing of hydroxyapatite-based materials is important for biomedical applications and this involves of need for familiarity and recognition of thermal stability and transitions during heating. Thermal treatment of HAp impacts in a series of physicochemical processes that depend on the receiving conditions of samples and extensively affect subsequent behaviour of the material [52].

In order to clarify all processes that can occur during heat treatment, thermal stability of HAp whiskers at elevated temperatures was investigated. On the DTA plots a broad peak in range of 400–1100 °C is visible. This peak consists of several peaks that correspond to different overlapping processes. First process (around 400–630 °C) is connected with the water loss within the network. It is lattice water, chemically bounded water inside the pore or released of chemisorped water [52, 53]. The second process (in a temperature of 885.7 °C and 885.9 °C for 3 h and 5 h synthesis respectively) is related to dehydroxylation [52, 53]. According to literature data [54] as the temperature increases, HAp loses OH$^-$ groups and gradually transforms into oxyhydroxyapatite (OHAp) and OHAp is transformed to oxyapatite (OAp). Dehydroxylation of hydroxyapatite starts at temperatures at about 900 °C in air and 850 °C in water-free atmosphere and occurs in two steps, in accordance with the reaction 1 and 2 [55]:

$$Ca_{10}(PO_4)_6(OH)_2 \rightarrow Ca_{10}(PO_4)_6(OH)_{2-2x}O_x\square_x + xH_2O \tag{1}$$

$$Ca_{10}(PO_4)_6(OH)_{2-2x}O_x\square_x \rightarrow Ca_{10}(PO_4)_6O + (1-x)H_2O \tag{2}$$

The hydroxyl ion-deficient product, $Ca_{10}(PO_4)_6(OH)_{2-2x}O_x$ $\square_x$ ($\square$ = a hydrogen vacancy, $x < I$) is known as oxyhydroxyapatite (OHAp), $Ca_{10}(PO_4)_6O$ is oxyapatite (OAp) [56].

Next, OAp decomposes above 1050 °C into a mixture of tetracalciumphosphate (TTCP) and tricalciumphosphate (TCP) in accordance with reactions (3) and (4) [52, 54]:

$$Ca_{10}(PO_4)_6O \rightarrow 2Ca_3(PO_4)_2 + Ca_4(PO_4)_2O \tag{3}$$

$$Ca_{10}(PO_4)_6O \rightarrow 3Ca_3(PO_4)_2 + CaO \tag{4}$$

where $Ca_4(PO_4)_2O$ is TTCP and $Ca_3(PO_4)_2$ is TCP.

HAp can also decompose according to the reaction [52]:

$$Ca_{10}(PO_4)_6(OH)_2 \rightarrow 2Ca_3(PO_4)_2 + Ca_4(PO_4)_2O + H_2O \tag{5}$$
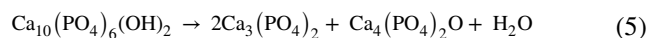
It's also known from literature data [57] that in the range of 890–1360 °C further dehydroxylation occurs. According to reaction (6) during the transformation of HAp to β-TCP additional water is produced. The loss of this water occurs between 850 and 1120 °C [57].

$$Ca_{10}(PO_4)_6(OH)_2 \rightarrow 3Ca_3(PO_4)_2 + CaO + H_2O \tag{6}$$
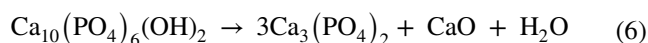
TCP has three polymorphic forms: β, α and α' [57]. The β-TCP form is stable up to 1125 °C and transforms to α-TCP form, which is stable in a temperature: 1125–1430 °C [54,

57], whereas. α'-TCP exists above 1430 °C [57]. As can be seen on Fig. 6 on DTA plot an endothermic peak connected with polymorphic transformation of α -TCP into α'-TCP in temperature around 1430 °C is visible. It's known that the α'-TCP polymorph spontaneously transforms to α-TCP on cooling and cannot be retained at room temperature even by quenching [57].

To confirm the processes occurred during thermal analysis, the phase composition of the residue from sample subjected to thermal stability tests was specified. XRD analysis confirmed the presence of HAp decomposition products. The XRD pattern of the sample after TG/DTA analysis, shows the presence of 30.3% of alpha-calcium phosphate (α-TCP) and 69.7% of tetracalcium phosphate (TTCP). The absence of characteristic signals for hydroxyapatite indicates its completely decomposition [42, 54].

## Conclusions

In this work, we focused on the synthesis with application with calcium lactate pentahydrate and orthophosphoric acid. HAp whiskers have been successfully synthesized with a facile and economic hydrothermal method with the use of cheap reactants, and simple experimental procedure. The effect of time of synthesis, the reaction heating rate, and stirring rate on hydroxyapatite composition and morphology was researched.

Hydrothermal method gives great opportunities for production of varied hydroxyapatite whiskers, which has importance for designing composite materials. Hydrothermal synthesis allows effective control of morphology of HAp by change in condition of synthesis.

This study presented the structural and thermal properties of synthetic samples containing HAp. The used SEM, FTIR, XRD and thermal analysis provides additional information about the samples and their composition. XRD analysis confirmed the presence of products of HAp decomposition. The XRD pattern of HAp sample after TG/DTA analysis shows the presence of 30.3% of α-TCP phase and 69.7% of TTCP phase. The morphology and crystallinity of the products depended on the synthesis temperature and time as well as the concentrations of soluble calcium and phosphate ions. The temperature, stirring rate and reaction heating rate had relatively little effect on the width of HAp whiskers.

The advantage of this presented method is obtaining pure hydroxyapatite of different morphology like whiskers, hexagonal rods and nano rods without the use of organic additives that can contaminate the product.

**Author's contributions** PS: corresponding author, contributed to conceptualization, methodology, design and preparation of synthesis, analysis and interpretation of data, manuscript writing, MB: analysis and interpretation of data, manuscript writing.

## Declarations

**Conflict of interest** The authors declare that they have no known competing financial interests or personal relationships that could have appeared to influence the work reported in this paper.

## References

1. Habraken W, Habibovic P, Epple M, Bohner M. Calcium phosphates in biomedical applications: materials for the future? Mater Today. 2016;19:69–87. https://doi.org/10.1016/j.mattod.2015.10.008.

2. Dorozhkin SV. Calcium orthophosphate bioceramics. Ceram Int. 2015;41:3913–66. https://doi.org/10.1016/j.ceramint.2015.08.004.

3. Šupová M. Substituted hydroxyapatites for biomedical applications: a review. Ceram Int. 2015;41:9203–31. https://doi.org/10.1016/j.ceramint.2015.03.316.

4. Bose S, Banerjee A, Dasgupta S, Bandyopadhyay A. Synthesis, processing, mechanical, and biological property characterization of hydroxyapatite whisker-reinforced hydroxyapatite composites. J Am Ceram Soc. 2009;92(2):323–30. https://doi.org/10.1111/j.1551-2916.2008.02881.x.

5. Zhang H, Darvell BW. Constitution and morphology of hydroxyapatite whiskers prepared using amine additives. J Eur Ceram Soc. 2010;30:2041–8. https://doi.org/10.1016/j.jeurceramsoc.2010.04.013.

6. Suchanek K, Bartkowiak A, Perzanowski M, Marszałek M. From monetite plate to hydroxyapatite nanofibers by monoethanolamine assisted hydrothermal approach. Sci Rep. 2018;8:1–9. https://doi.org/10.1038/s41598-018-33936-4.

7. Szcześ A, Hołysz L, Chibowski E. Synthesis of hydroxyapatite for biomedical applications. Adv Colloid Interface Sci. 2017;249:321–30. https://doi.org/10.1016/j.cis.2017.04.007.

8. Ghiasi B, Sefidbakht Y, Rezaei M. Hydroxyapatite for biomedicine and drug delivery. In: Rahmandoust M, Ayatollahi M, editors. Nanomaterials for advanced biological applications. Advanced structured materials, vol. 104. Cham: Springer; 2019. p. 85–120. https://doi.org/10.1007/978-3-030-10834-2_4.

9. Madhumathi K, Rubaiya Y, Doble M, Venkateswari R, Sampath Kumar TS. Antibacterial, anti-inflammatory, and bone-regenerative dual-drug-loaded calcium phosphate nanocarriers—in vitro and in vivo studies. Drug Deliv and Transl Res. 2018;8:1066–77. https://doi.org/10.1007/s13346-018-0532-6.

10. Xu YJ, Dong L, Zhang LCh, An D, Gao HL, Yang DM, Hu W, Sui C, Xu WP, Yu SH. Magnetic hydroxyapatite nanoworms for magnetic resonance diagnosis of acute hepatic injury. Nanoscale. 2016;8:84–1690. https://doi.org/10.1039/C5NR07023F.

11. Zhang D, Zhao H, Zhao X, Liu Y, Chen H, Li X. Application of hydroxyapatite as catalyst and catalyst carrier. Prog Chem. 2011;23:687–94.

12. Milovac D, Weigand I, Kovačić M, Ivanković M, Ivanković H. Highly porous hydroxyapatite derived from cuttlefish bone as TiO$_2$ catalyst support. Process Appl Ceram. 2018;12(2):136–42. https://doi.org/10.2298/PAC1802136M.

13. Amaechi BT, AbdulAzees PA, Alshareif DO, Shehata MA, de Carvalho Sampaio Lima PP, Abdollahi A, Kalkhorani PS, Evans V. Comparative efficacy of a hydroxyapatite and a fluoride toothpaste for prevention and remineralization of dental caries in children. BDJ Open. 2019;5:1–9. https://doi.org/10.1038/s41405-019-0026-8.

14. Dudek A, Adamczyk L. Properties of hydroxyapatite layers used for implant coatings. Opt Appl. 2013;XLIII(1):143–51. https://doi.org/10.5277/oa30118.

15. Le DT, Le TPT, Do HT, Vo HT, Pham NT, Nguyen TT, Cao HT, Nguyen PT, Dinh MT, Le HV, Tran DL. Fabrication of porous hydroxyapatite granules as an effective adsorbent for the removal of aqueous Pb(II) ions. J Chem. 2019. https://doi.org/10.1155/2019/8620181.

16. Biedrzycka A, Skwarek E, Hanna UM. Hydroxyapatite with magnetic core: synthesis methods, properties, adsorption and medical applications. Ad Colloi Interface Sci. 2021;291(102401):1–21. https://doi.org/10.1016/j.cis.2021.102401.

17. Holopainen J, Ritala M. Rapid production of bioactive hydroxyapatite fibers via electroblowing. J Eur Ceram Soc. 2016;36:3219–24. https://doi.org/10.1016/j.jeurceramsoc.2016.05.011.

18. Kasuga T, Ota Y, Nogami M, Abe Y. Preparation and mechanical properties of polylactic acid composites containing hydroxyapatite fibers. Biomaterials. 2001;22:19–23. https://doi.org/10.1016/S0142-9612(00)00091-0.

19. Roeder RK, Sproul MM, Turner CH. Hydroxyapatite whiskers provide improved mechanical properties in reinforced polymer composites. J Biomed Mater Res Part A. 2003;67(3):801–12. https://doi.org/10.1002/jbm.a.10140.

20. Zhang H, Zhang M, Shen Y, Pan H, Zhang K, Lu WW. Biocompatibility and bioactivity of hydroxyapatite whiskers reinforced bis-GMA based composites. In: 2010 3rd international conference on biomedical engineering and informatics, Yantai; 2010. p. 1640–4. https://doi.org/10.1109/BMEI.2010.5639603

21. Zhang C, Uchikoshi T, Liu L, Kikuchi M, Ichinose I. Nest-like microstructured biocompatible membrane fabricated by hydrothermally-synthesized hydroxyapatite (HAp) whiskers. J Eur Ceram Soc. 2020;40:513–20. https://doi.org/10.1016/j.jeurceramsoc.2019.09.032.

22. Aizawa M, Ueno H, Itatani K, Okada I. Syntheses of calcium-deficient apatite fibres by a homogeneous precipitation method and their characterizations. J Eur Ceram Soc. 2006;26:501–7. https://doi.org/10.1016/j.jeurceramsoc.2005.07.007.

23. You-fa W, Yu-hua Y, Hong-lian D, Mei-juan L. Preparation of hydroxyapatite fibers by the homogeneous precipitation method. J Wuhan Univ Technol-Mater Sci Ed. 2002;17(3):39–41. https://doi.org/10.1007/BF02838536.

24. Arce H, Montero ML, Sáenz A, Castañod VM. Effect of pH and temperature on the formation of hydroxyapatite at low temperatures by decomposition of a Ca–EDTA complex. Polyhedron. 2004;23(11):1897–901. https://doi.org/10.1016/j.poly.2004.04.021.

25. Kandori K, Horigami N, Yasukawa A, Ishikawa T. Texture and formation mechanism of fibrous calcium hydroxyapatite particles prepared by decomposition of calcium–EDTA chelates. J Am Ceram Soc. 1997;80:1157–64. https://doi.org/10.1111/j.1151-2916.1997.tb02958.x.

26. Seo DS, Lee JK. Synthesis of hydroxyapatite whiskers through dissolution–reprecipitation process using EDTA. J Cryst Growth. 2008;310:2162–7. https://doi.org/10.1016/j.jcrysgro.2007.11.028.

27. Yoon SY, Park YM, Park SS, Stevens R, Park HC. Synthesis of hydroxyapatite whiskers by hydrolysis of α-tricalcium phosphate using microwave heating. Mater Chem Phys. 2005;91:48–53. https://doi.org/10.1016/j.matchemphys.2004.10.049.

28. Mizutania Y, Hattoria M, Okuyama M, Kasuga HC, Nogami M. Large-sized hydroxyapatite whiskers derived from calcium tripolyphosphate gel. J Eur Ceram Soc. 2005;25:3181–5. https://doi.org/10.1016/j.jeurceramsoc.2004.07.028.

29. Suchanek W, Suda H, Yashima M, Kakihana M, Yoshimura M. Biocompatible whiskers with controlled morphology and stoichiometry. J Mater Res. 1996;10(3):521–9. https://doi.org/10.1557/JMR.1995.0521.

30. Yoshimura M, Suda H, Okamoto K, Ioku K. Hydrothermal synthesis of biocompatible whiskers. J Mater Sci. 1994;29:3399–402. https://doi.org/10.1007/BF00352039.

31. Zhang H, Darvell BW. Formation of hydroxyapatite whiskers by hydrothermal homogeneous precipitation using acetamide. J Am Ceram Soc. 2011;94(7):2007–13. https://doi.org/10.1111/j.1551-2916.2010.04338.x.

32. Khalameida S, Sydorchuk V, Skubiszewska-Zięba J, Charmas B, Skwarek E, Janusz W. Hydrothermal, microwave and mechanochemical modification of amorphous zirconium phosphate structure. J Therm Anal Calorim. 2017;128:795–806. https://doi.org/10.1007/s10973-016-5965-x.

33. Cao X, Wang G, Yang Y, Cao Y, Cao X. Biomolecules induce the synthesis of hollow hierarchical mesoporous structured hydroxyapatite microflowers: application in macromolecule drug delivery. J Mater Sci. 2021;56:7034–49. https://doi.org/10.1007/s10853-020-05688-y.

34. Zhang H, Darwell BW. Morphology and structural characteristics of hydroxyapatite whiskers: effect of the initial Ca concentration, Ca/P ratio and pH. Acta Biomater. 2011;7(7):2960–8. https://doi.org/10.1016/j.actbio.2011.03.020.

35. Zhang H. Effect of synthesis temperature on morphology and structural characteristics of hydroxyapatite whiskers. Ceramics-Silikáty. 2018;62(2):181–7. https://doi.org/10.13168/cs.2018.0010.

36. Iizuka T. Effects of pH of the aqueous solutions on the growth of hydroxyapatite whiskers. J Ceram Soc JPN. 2008;106(8):820–3. https://doi.org/10.2109/jcersj.106.820.

37. Lin K, Wu C, Chang J. Advances in synthesis of calcium phosphate crystals with controlled size and shape. Acta Biomater. 2014;10(10):4071–102. https://doi.org/10.1016/j.actbio.2014.06.017.

38. Roeder RK, Converse GL, Leng H, Yue W. Kinetic effects on hydroxyapatite whiskers synthesized by the chelate decomposition method. J Am Ceram Soc. 2006;89(7):2096–104. https://doi.org/10.1111/j.1551-2916.2006.01067.x.

39. György S, Károly Z, Fazekas P, Németh P, Bódis E, Menyhárd A, Kótai L, Klébert S. Effect of the reaction temperature on the morphology of nanosized HAp. J Therm Anal Calorim. 2019;138:145–51. https://doi.org/10.1007/s10973-019-08255-z.

40. Szterner P, Biernat M. The synthesis of hydroxyapatite by hydrothermal process with calcium lactate pentahydrate: the effect of reagent concentrations, pH, temperature, and pressure. Bioinorg Chem Appl. 2022;3481677:1–13. https://doi.org/10.1155/2022/3481677.

41. Peña J, Vallet-Regi M. Hydroxyapatite, tricalcium phosphate and biphasic materials prepared by a liquid mix technique. J Eur Ceram Soc. 2003;23:1687–96. https://doi.org/10.1016/S0955-2219(02)00369-2.

42. Carrodeguas RG, De Aza S. α-Tricalcium phosphate: synthesis, properties and biomedical applications. Acta Biomater. 2011;7:3536–46. https://doi.org/10.1016/j.actbio.2011.06.019.

43. Ebrahimi M, Botelho MG, Dorozhkin SV. Biphasic calcium phosphates bioceramics (HA/TCP): concept, physicochemical properties and the impact of standardization of study protocols in biomaterials research. Mater Sci Eng C. 2017;71(1):1293–312. https://doi.org/10.1016/j.msec.2016.11.039.

44. Chen J, Liu J, Deng H, Yao S, Wang S. Regulatory synthesis and characterization of hydroxyapatite nanocrystals by a microwave-assisted hydrothermal method. Ceram Int. 2019;46(2):2185–93. https://doi.org/10.1016/j.ceramint.2019.09.203.

45. Koutsopoulos S. Synthesis and characterization of hydroxyapatite crystals: a review study on the analytical methods. J Biomed Mater Res. 2002;62(4):600–12. https://doi.org/10.1002/jbm.10280.

46. Oancea A, Grasset O, Le Menn E, Bollengier O, Bezacier L, Le Mouélic S, Tobie G. Laboratory infrared reflection spectrum of carbon dioxide clathrate hydrates for astrophysical remote sensing applications. Icarus. 2012;221(2):900–10. https://doi.org/10.1016/j.icarus.2012.09.020.

47. Mathew M, Schroeder W, Dickens B, Brown WE. The crystal structure of alpha-$Ca_3(PO_4)_2$. Acta Crystallogr B. 1977;33:1325–33. https://doi.org/10.1107/S0567740877006037.

48. Dickens B, Brown WE, Kruger GJ, Stewart JM. $Ca_4(PO_4)_2O$, tetracalcium diphosphate monoxide. Crystal structure and relationships to $Ca_5(PO_4)_3OH$ and $K_3Na(SO_4)_2$. Acta Cryst. 1973;B29:2046–56. https://doi.org/10.1107/S0567740873006102.

49. Wang S, Wang Y, Sun K, Sun X. Low temperature preparation of α-tricalcium phosphate and its mechanical properties. Process Appl Ceram. 2017;11(2):100–5. https://doi.org/10.2298/PAC1702100W.

50. Durucan C, Brown PW. Reactivity of α-tricalcium phosphate. J Mater Sci. 2002;37(5):963–9. https://doi.org/10.1023/A:1014347814241.

51. De Oliveira JF, De Aguiar PF, Rossi AM, Soares GA. Effect of process parameters on the characteristics of porous calcium phosphate ceramics for bone tissue scaffolds. Artif Organs. 2003;27(5):406–11. https://doi.org/10.1046/j.1525-1594.2003.07247.x.

52. Sofronia AM, Baies R, Anghel EM, Marinescu CA, Tanasescu S. Thermal and structural characterization of synthetic and natural nanocrystalline hydroxyapatite. Mater Sci Eng C. 2014;43:153–63. https://doi.org/10.1016/j.msec.2014.07.023.

53. Kohutová A, Honcová P, Svoboda L, Bezdička P, Mařiková M. Structural characterization and thermal behaviour of biological hydroxyapatite. J Therm Anal Calorim. 2012;108(1):163–70. https://doi.org/10.1007/s10973-011-1942-6.

54. Tõnsuaadu K, Goss KA, Pludums L, Veiderma M. A review on the thermal stability of calcium apatites. J Therm Anal Calorim. 2012;110(2):647–59. https://doi.org/10.1007/s10973-011-1877-y.

55. Matraszek A, Radomińska E. The revised phase diagram of the $Ca_3(PO_4)_2$–$YPO_4$ system. The temperature and concentration range of solid-solution phase fields. J Therm Anal Calorim. 2014;117:101–8. https://doi.org/10.1007/s10973-014-3662-1.

56. Wang PE, Chaki TK. Sintering behaviour and mechanical properties of hydroxyapatite and dicalcium phosphate. J Mater Sci: Mater Med. 1993;4:150–8. https://doi.org/10.1007/BF00120384.

57. Parthiban SP, Elayaraja K, Girija EK, Yokogawa Y, Kesavamoorthy R, Palanichamy M, Asokan K, Kalkura SN. Preparation of thermally stable nanocrystalline hydroxyapatite by hydrothermal method. J Mater Sci Mater Med. 2009;20:77–83. https://doi.org/10.1007/s10856-008-3484-4.